SANDIA REPORT
SAND2020-4015
Printed April 2020

Sandia National Laboratories

Benchmark problems for the Mesoscale Multiphysics Phase Field Simulator (MEMPHIS)

R. Dingreville, J.A. Stewart, E.Y. Chen

Prepared by
Sandia National Laboratories
Albuquerque, New Mexico 87185
Livermore, California 94550

Issued by Sandia National Laboratories, operated for the United States Department of Energy by National Technology & Engineering Solutions of Sandia, LLC.

Available to DOE and DOE contractors from

U.S. Department of Energy
Office of Scientific and Technical Information
P.O. Box 62
Oak Ridge, TN 37831

Telephone: (865) 576-8401
Facsimile: (865) 576-5728
E-Mail: reports@osti.gov
Online ordering: http://www.osti.gov/scitech

Available to the public from

U.S. Department of Commerce
National Technical Information Service
5301 Shawnee Road
Alexandria, VA 22312

Telephone: (800) 553-6847
Facsimile: (703) 605-6900
E-Mail: orders@ntis.gov
Online order: https://classic.ntis.gov/help/order-methods

ABSTRACT

This report details the current benchmark results to verify, validate and demonstrate the capabilities of the in-house multi-physics phase-field modeling framework **Me**soscale **M**ultiphysics **Ph**ase F**i**eld **S**imulator (MEMPHIS) developed at the Center for Integrated Nanotechnologies (CINT). MEMPHIS is a general phase-field capability to model various nanoscience and materials science phenomena related to microstructure evolution. MEMPHIS has been benchmarked against a suite of reported 'classical' phase-field benchmark problems to verify and validate the correctness, accuracy and precision of the models and numerical methods currently implemented into the code.

ACKNOWLEDGMENT

This work was performed at the Center for Integrated Nanotechnologies, an Office of Science User Facility operated for the U.S. Department of Energy.

CONTENTS

1. Introduction **9**

2. Benchmark problem: Spinodal Decomposition **10**
- 2.1. Free energy evolution 10
- 2.2. Final microstructure 11
- 2.3. Computational efficiency 11

3. Benchmark problem: Dendritic Growth **14**
- 3.1. Free energy evolution 14
- 3.2. Solid fraction evolution 14
- 3.3. Solid-liquid boundary and tip position evolution 15
- 3.4. Computational efficiency 15

4. Benchmark problem: Elasticity **17**
- 4.1. Free energy and elastic energy evolution 17
- 4.2. Precipitate length evolution and precipitate boundary at equilibrium 17
- 4.3. Computational efficiency 17

5. Benchmark problem: Manufactured Solutions **21**
- 5.1. Spatial accuracy 21

6. Benchmark problem: Thermal Diffusion **23**
- 6.1. Implementation of Thermal Diffusion 23
- 6.2. Temperature profiles at steady-state 25

7. Summary **26**

References **27**

LIST OF FIGURES

Figure 2-1. Evolution of the free energy for the spinodal decomposition model with (a) periodic boundary conditions and (b) no-flux boundary conditions. 11
Figure 2-2. Microstructure evolution as a function of time for periodic boundary conditions (first column) and no-flux boundary conditions (second column) using explicit Euler integration. 12
Figure 2-3. Computational efficiency for the various numerical methods implemented into MEMPHIS for the spinodal decomposition model. 13

Figure 3-1. Evolution of the free energy for the dendritic growth model. 15
Figure 3-2. Evolution of the solid fraction in the domain for the dendritic growth model. . . . 15
Figure 3-3. Evolution of (a) the solidification profile at various time, and (b) the dendrite tip position versus time for the dendritic growth model. 16
Figure 3-4. Computational efficiency for the various numerical methods implemented into MEMPHIS for the dendritic growth model. 16

Figure 4-1. Evolution of the free energy of a constrained precipitate with a radius of $r =$ 20 nm ((a) and (c)) and $r = 75$ nm ((b) and (d)), when the precipitate elastic stiffness is the same as the matrix ((a) and (b)), and when the precipitate elastic stiffness is 1.1 stiff than that in the matrix. 18
Figure 4-2. The precipitate lengths along the [10], [01] and diagonal directions, respectively, measured from the center of the drop to the contour in the x ([10]), y ([01]) and diagonal directions. The angle used for the diagonal direction is given by θ_d such that $\tan\theta_d = a_{01}/a_{10}$. 19
Figure 4-3. Precipitate boundary at equilibrium for cases with a radius of $r = 20$ nm ((a) and (c)) and $r = 75$ nm ((b) and (d)), when the precipitate elastic stiffness is the same as the matrix ((a) and (b)), and when the precipitate elastic stiffness is 1.1 stiff than that in the matrix. 20

Figure 5-1. Spatial accuracy for MEMPHIS three sets of tests to conduct using the Method of Manufactured Solutions (MMS) problem. The primary purpose of the first test is provide a computationally inexpensive problem to verify a simulation code. The second and third tests are more computationally demanding and are primarily designed to serve as a basis for performance comparisons. 22

Figure 6-1. Schematics of 1D plane wall problems. a) Plane wall with fixed temperature of T_1 at $x = 0$ and T_2 at $x = L$. b) Plane wall with an uniform heat source $\dot{q}$, adiabatic surface at $x = 0$ and free surface at $x = L$ with a temperature of T_s and outward flux of q". The variable k represents the constant thermal conductivity. 24

Figure 6-2. Temperature profile across the computational domain at steady-state in the case of (a) the 1D-plane wall with different fixed temperatures and, (b) the 1D-plane wall with a heat source. 25

LIST OF TABLES

1. INTRODUCTION

An in-house multi-physics phase-field modeling capability entitled **Me**soscale **M**ultiphysics **Ph**ase F**i**eld **S**imulator (MEMPHIS) has been developed at the Center for Integrated Nanotechnologies (CINT) in order to model various nanoscience and materials science phenomena related to microstructure evolution. MEMPHIS is written in modular Fortran to enable rapid model development and prototyping, and performs 2D and 3D calculations in serial or in parallel using message-passing techniques and spatial decomposition of the computational domain. The modular framework of MEMPHIS is designed such that any user can focus solely on the development and implementation of a self-contained physics-based model without the need for extensive software-development experience to seamlessly integrate a user's model in MEMPHIS. The current capability (i.e., 2019) comprises a spinodal decomposition model, dendritic growth model, a physical vapor deposition model, a quantum dot growth model, and a linear elasticity model. Details can be found in the manuscript by Stewart and Dingreville [7].

The current version of the code can be requested from the corresponding author (rdingre@sandia.gov) and is distributed at the discretion of Sandia National Laboratories through the Center for Integrated Nanotechnologies (CINT) User Program.

In order to validate both the correctness of the numerical methods and models, along with the overall capabilities implemented in MEMPHIS, we utilized published phase-field benchmark problems to verify and validate every component of this phase-field capability. These benchmark problems are described elsewhere [4, 5] and are available on the National Institute of Standards and Technology (NIST) "PFHub" repository website (`https://pages.nist.gov/pfhub/`). The benchmark problems used to validate the methods directly relevant to the models currently implemented in MEMPHIS are (i) spinodal decomposition to test the Cahn-Hilliard solutions (see Section 2), (ii) dendrite growth to test the solutions of coupled differential equations (see Section 3), (iii) linear elasticity of a constrained precipitate to test the elasticity model (see Section 4), (iv) the method of manufactured solutions (MMS) to test the various numerical integration schemes implemented in the MEMPHIS framework (see Section 5), namely explicit Euler, midpoint method, and the iterative Heun's method, and (v) a thermal diffusion (see Section 6) to test the implicit vs. explicit integration schemes. Note that this last benchmark problem is not part of the benchmark problems available on the "PFHub" repository website. Each result obtained with MEMPHIS has been verified and validated with satisfactory agreement with existing benchmark solutions, providing quality assurance on the validity, performance and accuracy of MEMPHIS capabilities. Our results (except the thermal diffusion problem) are available on the NIST website for comparison against the existing benchmark solutions.

2. BENCHMARK PROBLEM: SPINODAL DECOMPOSITION

This benchmark problem looks into the classical spinodal decomposition microstructure evolution problem. Spinodal decomposition is one of the oldest problems in phase-field and goes back to the seminal works by Cahn and Hilliard [1]. While spinodal decomposition may be one of the simplest phase-field model, it is highly relevant, as a large number of phase-field models include the diffusion of a solute within a matrix. Furthermore, precipitation and growth may also be modeled with the same formulation if the appropriate initial conditions are chosen. Here, we benchmarked MEMPHIS against this simple formulation that is numerically tractable so that results may be obtained quickly and interpreted easily, testing the essential physics while minimizing model complexity and the chance to introduce coding errors.

The two benchmark problems tested here correspond to square computational domains with side length of 200 units (dimensionless). In one case, periodic boundary conditions are applied to a square domain (problem 1(a)), while. in the other case, no-flux boundaries are applied to a square domain (problem 1(b)). Note that the same initial conditions are used for the square computational domains with periodic boundary or no-flux boundary conditions, such that when periodic boundary conditions are applied, there is a discontinuity in the initial condition at the domain boundaries. Description of the spinodal model is described elsewhere [4]. Parametrization and simulation conditions are described at
`https://pages.nist.gov/pfhub/benchmarks/benchmark1.ipynb/`

Three metrics are required for these two benchmark problems:

1. the evolution of the free energy as a function of the computational time;
2. the final microstructure; and
3. the computational efficiency (Memory used vs. Wall-clock time/Simulation end time).

2.1. FREE ENERGY EVOLUTION

Figure 2-1 shows the evolution of the free energy as a function of the computational time for the three numerical methods (i.e., explicit Euler, Heuns, midpoint methods) implemented in MEMPHIS. All three numerical methods for time integration lead to similar results regardless of the boundary conditions used. These results are in good agreement with those posted on the NIST "PFHub" repository website.

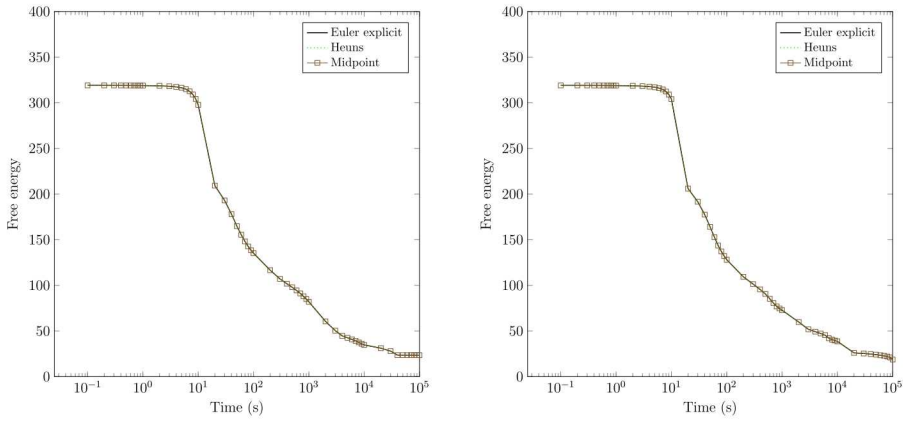

(a) Periodic boundary (b) No-flux boundary

Figure 2-1. Evolution of the free energy for the spinodal decomposition model with (a) periodic boundary conditions and (b) no-flux boundary conditions.

2.2. FINAL MICROSTRUCTURE

Figure 2-2 shows the time evolution of the spinodal decomposition microstructure for the periodic and no-flux boundary conditions when using the Euleer explicit method. All three numerical methods (explicit Euler, Heuns, midpoint methods) lead to similar microstructure evolutions. These results are in good agreement with those posted on the NIST "PFHub" repository website.

2.3. COMPUTATIONAL EFFICIENCY

Figure 2-3 shows the computational efficiency for the various numerical methods (explicit Euler, Heuns, midpoint methods) implemented in MEMPHIS. These results show comparable performances with other phase-field code performance posted on the NIST "PFHub" repository website.

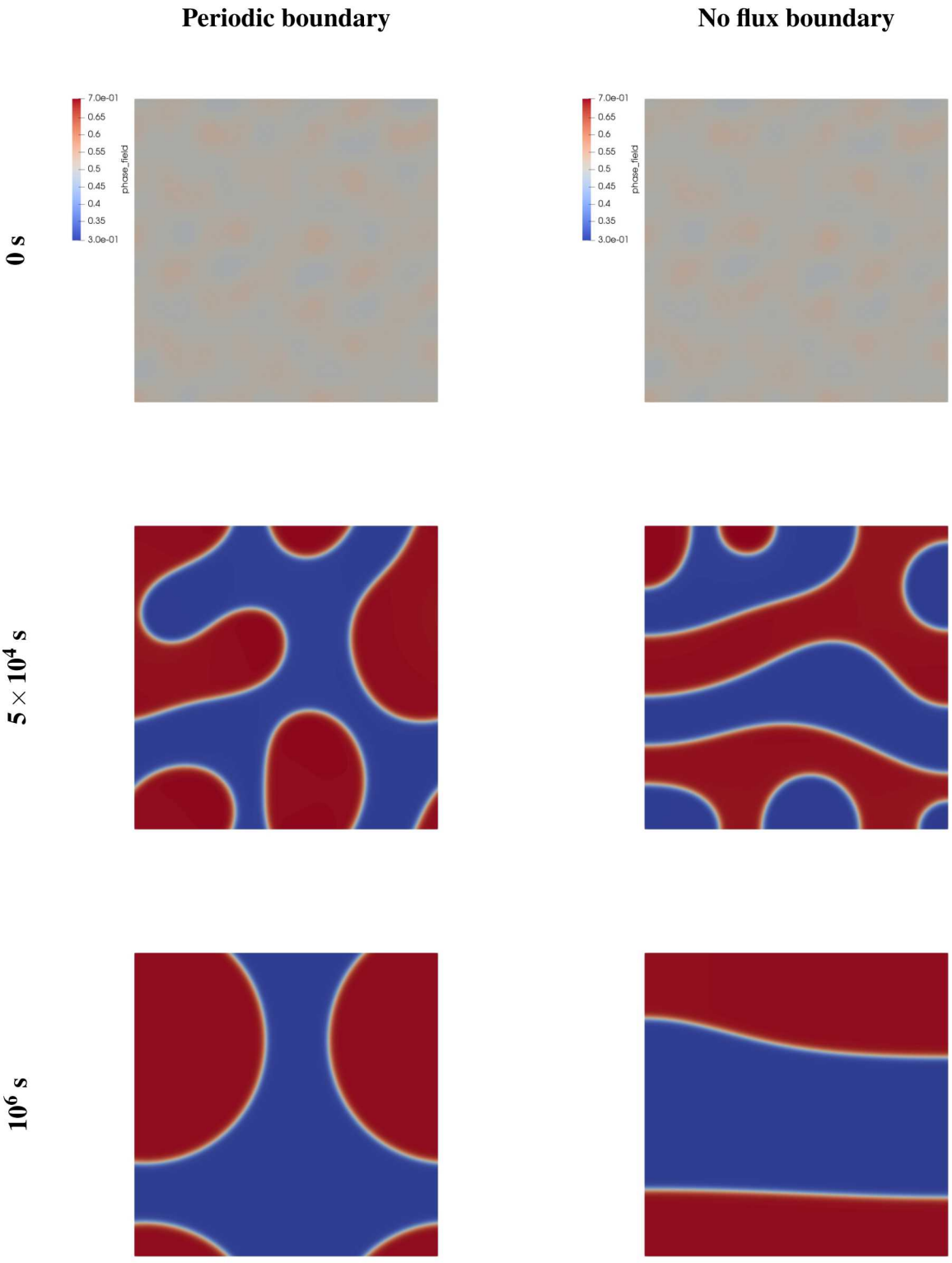

Figure 2-2. Microstructure evolution as a function of time for periodic boundary conditions (first column) and no-flux boundary conditions (second column) using explicit Euler integration.

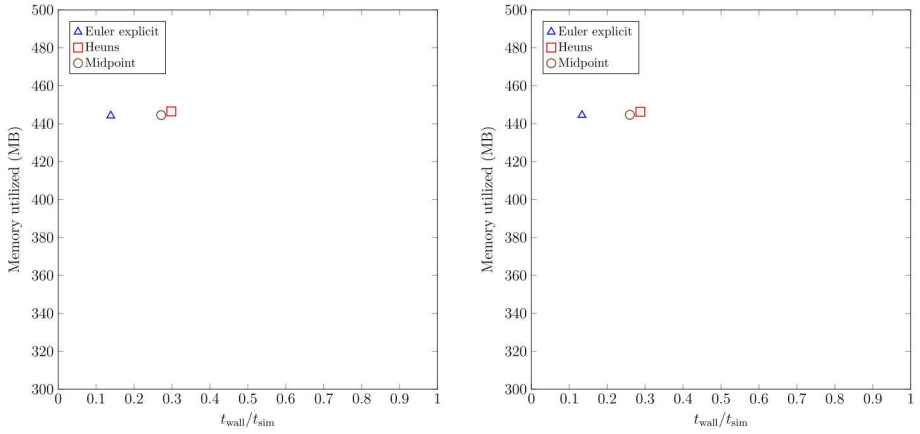

(a) Periodic boundary (b) No-flux boundary

Figure 2-3. Computational efficiency for the various numerical methods implemented into MEMPHIS for the spinodal decomposition model.

3. BENCHMARK PROBLEM: DENDRITIC GROWTH

This benchmark problem looks into dendritic growth simulations. Dendritic growth simulations are useful as benchmark problems since these simulations are highly sensitive to both the phase-field model formulation and the particular numerical implementation employed. The model for solidification and dendritic growth incorporates anisotropic interfacial energy and the release of latent heat. Description of the dendritic model is described in [5, 6]. Parametrization and simulation conditions are described at
https://pages.nist.gov/pfhub/benchmarks/benchmark3.ipynb/

Four metrics are required for this benchmark problem:

1. the solid fraction in the domain;
2. the free energy;
3. the estimated tip position versus time; and
4. the computational efficiency.

3.1. FREE ENERGY EVOLUTION

Figure 3-1 shows the evolution of the free energy as a function of the computational time for the three numerical methods (i.e., explicit Euler, Heuns, midpoint methods) implemented into MEMPHIS. All three numerical methods for time integration lead to similar results. These results are in good agreement with those posted on the NIST "PFHub" repository website for this problem.

3.2. SOLID FRACTION EVOLUTION

Figure 3-2 shows the evolution of the solid fraction in the domain as a function of the computational time for the three numerical methods (i.e., explicit Euler, Heuns, midpoint methods) implemented into MEMPHIS. These results are in good agreement with those posted on the NIST "PFHub" repository website for this problem.

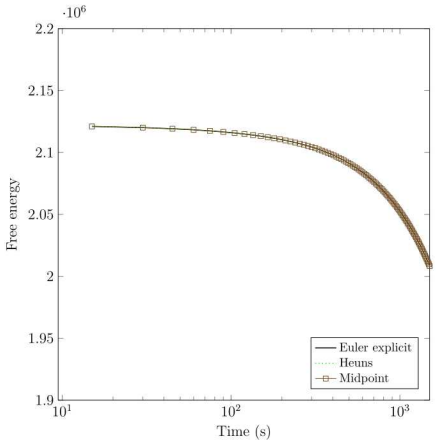

Figure 3-1. Evolution of the free energy for the dendritic growth model.

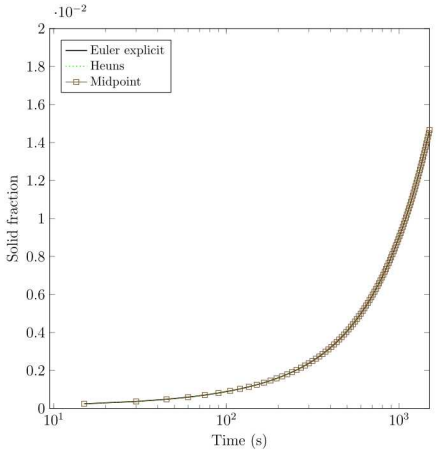

Figure 3-2. Evolution of the solid fraction in the domain for the dendritic growth model.

3.3. SOLID-LIQUID BOUNDARY AND TIP POSITION EVOLUTION

Figure 3-3 shows evolution of the solid-liquid boundary (Fig. 3-3 (a)) and the tip position (Fig. 3-3 (b)) for the explicit Euler numerical method. These results are in good agreement with those posted on the NIST "PFHub" repository website for this problem.

3.4. COMPUTATIONAL EFFICIENCY

Figure 3-4 shows the computational efficiency for the various numerical methods (explicit Euler, Heuns, midpoint methods) implemented in MEMPHIS. These results show comparable

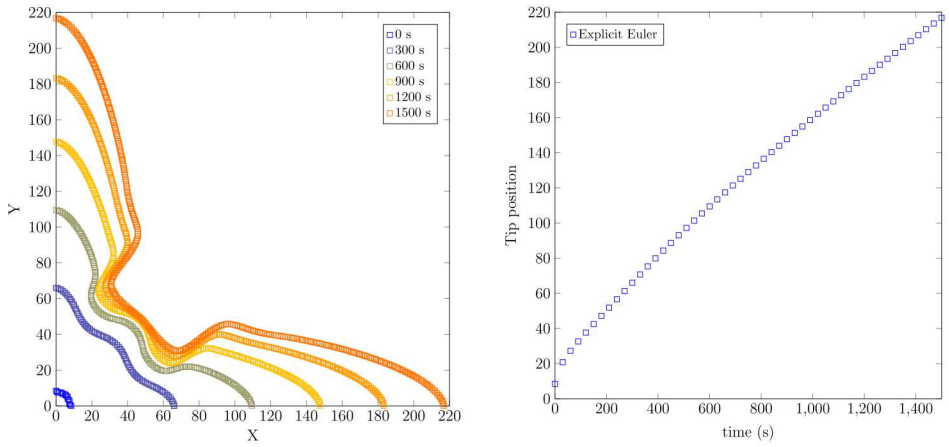

(a) Solid-liquid boundary (b) Tip position

Figure 3-3. Evolution of (a) the solidification profile at various time, and (b) the dendrite tip position versus time for the dendritic growth model.

performances with other phase-field code performance posted on the NIST "PFHub" repository website.

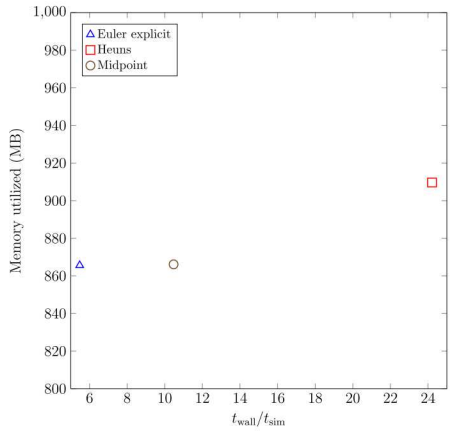

Figure 3-4. Computational efficiency for the various numerical methods implemented into MEMPHIS for the dendritic growth model.

4. BENCHMARK PROBLEM: ELASTICITY

This benchmark problem looks into (a) a coherent precipitate elastically stressed if a lattice parameter is mismatched between the matrix and precipitate phases, or (b) a volumetric elastic stresses arise for an incoherent precipitate due to thermal expansion mismatch with the matrix. The model for an elastically constrained precipitate adds the physics of linear elastic solid mechanics to the Cahn-Hilliard equation. Four different parameter variations for this problem are studies: two precipitate radius, and two elasticity stiffness tensors. Description of the elasticity model is described in [3, 5]. Parametrization and simulation conditions are described at `https://pages.nist.gov/pfhub/benchmarks/benchmark4.ipynb/`

Five metrics are required for this benchmark problem:

1. the total free energy in the domain;
2. the interfacial free energy;
3. the elastic free energy;
4. the area of the precipitate; and
5. the precipitate lengths measured from the center of the drop to a specified contour.

4.1. FREE ENERGY AND ELASTIC ENERGY EVOLUTION

Figure 4-3 shows the evolution of the free energy, elastic energy and interfacial free energy as a function of the computational time for the four cases studied using MEMPHIS. All three numerical methods for time integration lead to similar results regardless of the boundary conditions used. These results are in good agreement with those posted on the NIST "PFHub" repository website.

4.2. PRECIPITATE LENGTH EVOLUTION AND PRECIPITATE BOUNDARY AT EQUILIBRIUM

4.3. COMPUTATIONAL EFFICIENCY

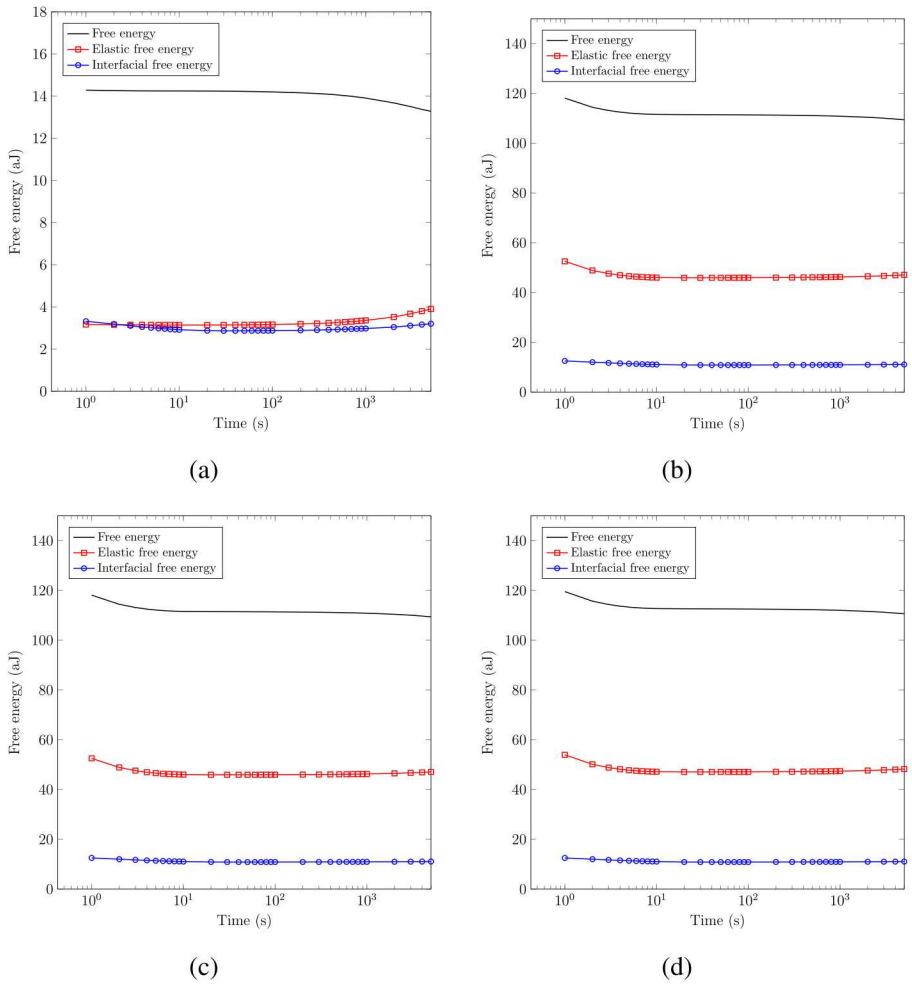

Figure 4-1. Evolution of the free energy of a constrained precipitate with a radius of $r = 20$ nm ((a) and (c)) and $r = 75$ nm ((b) and (d)), when the precipitate elastic stiffness is the same as the matrix ((a) and (b)), and when the precipitate elastic stiffness is 1.1 stiff than that in the matrix.

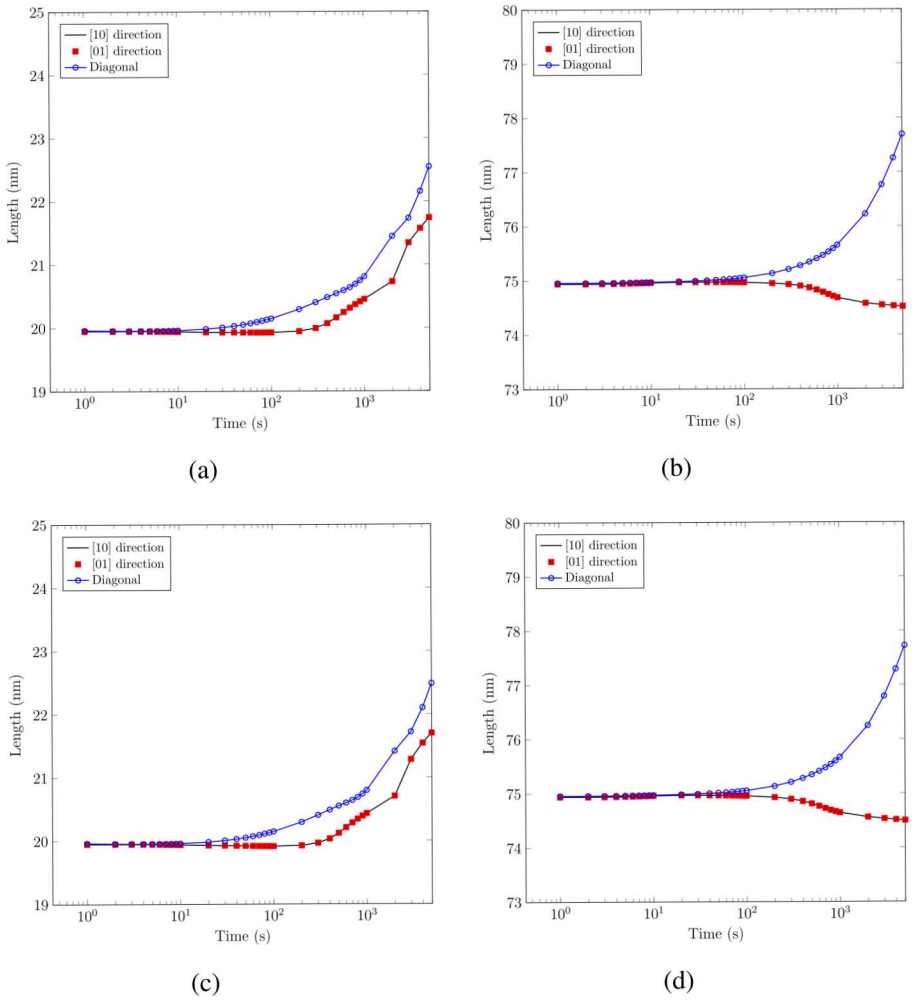

Figure 4-2. The precipitate lengths along the [10], [01] and diagonal directions, respectively, measured from the center of the drop to the contour in the x ([10]), y ([01]) and diagonal directions. The angle used for the diagonal direction is given by θ_d such that $\tan\theta_d = a_{01}/a_{10}$.

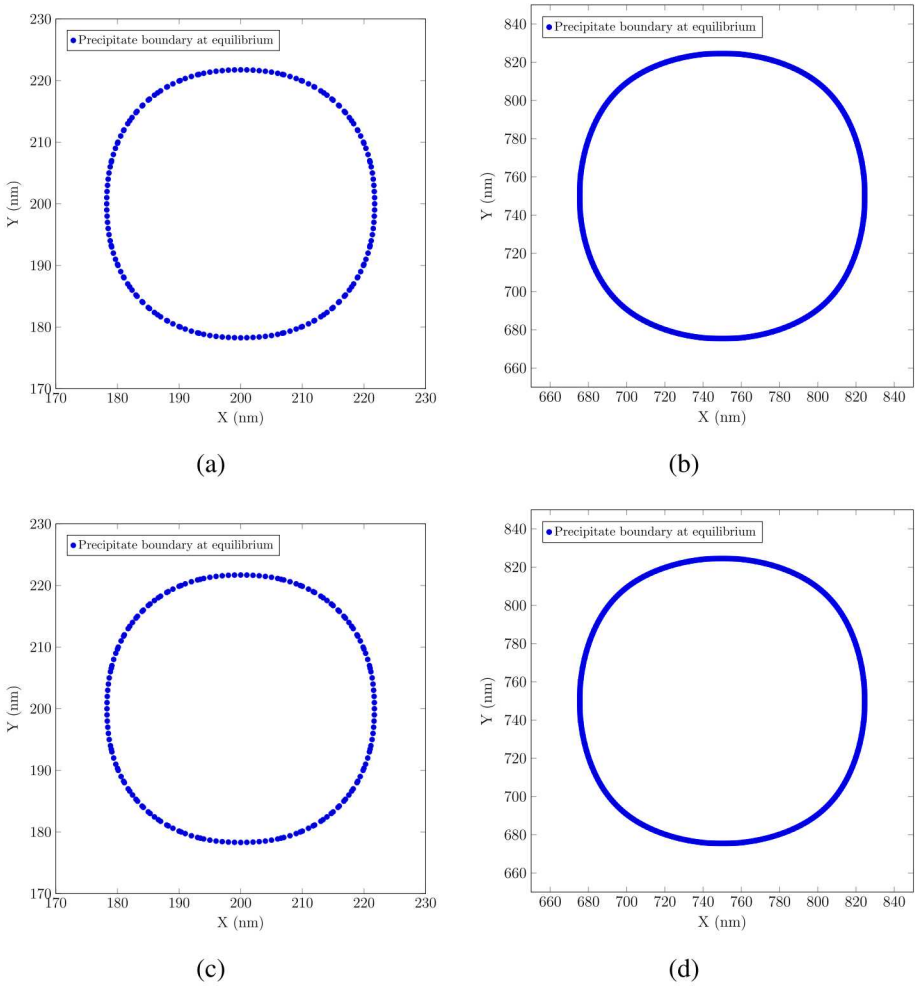

Figure 4-3. Precipitate boundary at equilibrium for cases with a radius of $r = 20$ nm ((a) and (c)) and $r = 75$ nm ((b) and (d)), when the precipitate elastic stiffness is the same as the matrix ((a) and (b)), and when the precipitate elastic stiffness is 1.1 stiff than that in the matrix.

5. BENCHMARK PROBLEM: MANUFACTURED SOLUTIONS

This benchmark problem looks into the so-called "Method of Manufactured Solutions". MMS is a technique for verifying the accuracy of MEMPHIS. In the MMS, one picks a desired solution to the problem at the outset, the "manufactured solution", and then determines the governing equation that will result in that solution. With the exact analytical form of the solution in hand, when the governing equation is solved using a particular simulation code, the deviation from the expected solution can be determined exactly.

In this benchmark problem, the objective is to use the MMS to rigorously verify phase-field simulation codes and then provide a basis of comparison for the computational performance between codes and for various settings for a single code. Parametrization and simulation conditions are described at
https://pages.nist.gov/pfhub/benchmarks/benchmark7.ipynb/

Two metrics are required for this benchmark problem:

1. Temporal accuracy of the numerical method; and
2. Spatial accuracy of the numerical method.

In the following only the results for the spatial accuracy will be presented for the time being.

5.1. SPATIAL ACCURACY

Figure 5-1 shows the order of spatial accuracy as compared to the theoretical order of accuracy for the numerical method employed in the simulation for benchmark problems 7(a), 7(b), and 7(c), respectively as described in the "PFHub" repository website. The primary purpose of the first test is provide a computationally inexpensive problem to verify a simulation code. The second and third tests are more computationally demanding and are primarily designed to serve as a basis for performance comparisons. These results show comparable performances with other phase-field code performance posted on the NIST "PFHub" repository website.

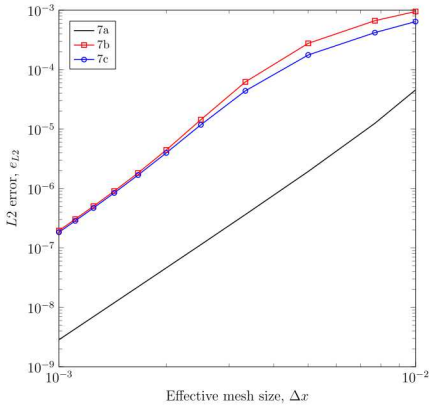

Figure 5-1. Spatial accuracy for MEMPHIS three sets of tests to conduct using the Method of Manufactured Solutions (MMS) problem. The primary purpose of the first test is provide a computationally inexpensive problem to verify a simulation code. The second and third tests are more computationally demanding and are primarily designed to serve as a basis for performance comparisons.

6. BENCHMARK PROBLEM: THERMAL DIFFUSION

This benchmark problem looks into the classical topic of thermal diffusion. Being of the most basic form of the diffusion problem, thermal diffusion is well studied and provides many analytical solutions that can be used to verify the correct implementation of the numerical solvers for implicit vs. explicit schemes. Coupling of a temperature field with a phase field can also provided additional details to thermal dependent processes such as solidification, melting and evaporation.

The current benchmark problem models two simplest cases of steady state thermal diffusion:

1. 1D-plane wall with different fixed temperatures on left and right boundaries; and
2. 1D-plane wall with a uniform heat source, adiabatic boundary on the left and free surface boundary on the right.

Diagram of these two cases can be found in Fig. 6-1.

The steady state temperature profile for Fig. 6-1(a) is straightforward. With the fixed temperature boundary conditions the system would eventually evolve into a linear gradient profile such that $T(x) = T_1 + x\frac{T_2 - T_1}{L}$. The steady state temperature profile for Fig. 6-1(b) is comparably more complex. Given that outward heat flux balances the uniform heat generation, i.e. $\dot{q} \times L = q$", the temperature profile would converge to $T(x) = \frac{\dot{q}L^2}{2k}(1 - \frac{x^2}{L^2}) + T_s$ [2].

In this benchmark problem, the objective is to use the 1D thermal diffusion problems to verify a basis of comparison between an explicit and an implicit integration scheme.

One metric is required for this benchmark problem:

1. Temperature profile across the computational domain.

6.1. IMPLEMENTATION OF THERMAL DIFFUSION

Implementation of the thermal diffusion problems follows the standard 3D thermal diffusion equation $\frac{\partial T}{\partial t} = \alpha(\nabla^2 T + \frac{\dot{q}}{k})$ where α is the thermal diffusivity. **In the explicit implementation**, the right-hand-side Laplacian is evaluated at the current frame such that $\frac{\partial T}{\partial t}$ can be independently solved at each grid point to evolve the system. In the present benchmark problem, the standard explicit Euler solver is used. **In the implicit implementation**, the right-hand-side Laplacian is

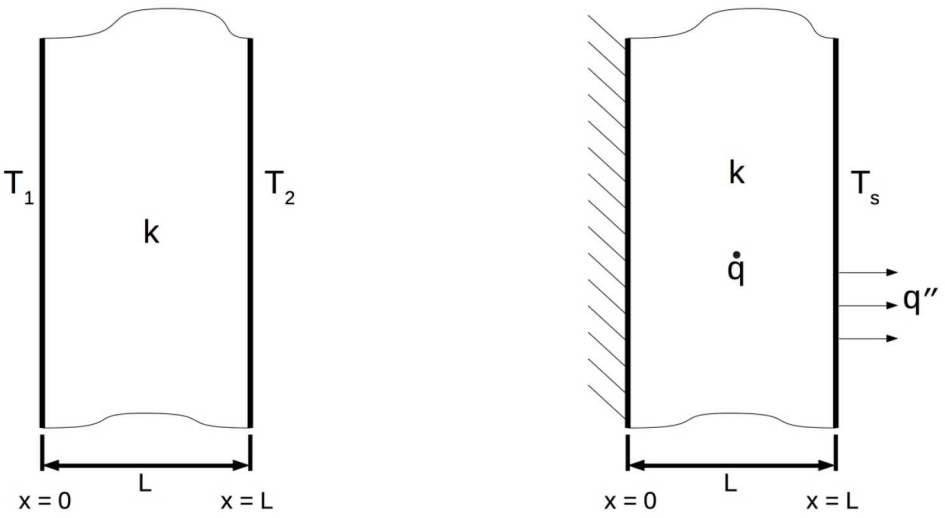

(a) (b)

Figure 6-1. Schematics of 1D plane wall problems. a) Plane wall with fixed temperature of T_1 at $x = 0$ and T_2 at $x = L$. b) Plane wall with an uniform heat source $\dot{q}$, adiabatic surface at $x = 0$ and free surface at $x = L$ with a temperature of T_s and outward flux of q". The variable k represents the constant thermal conductivity.

evaluated at t_{n+1} such that the entire temperature field T must be simultaneously solved through a system of equations or an iterative approach. For the results provided below, a red-black Gauss-Seidel [8] solver is implement to evolve the implicit systems to steady state.

Parametrization and simulation conditions are described below. Each pseudo-1D plane wall is constructed with $256 \times 16 \times 1$ grid size. In the Y and Z directions, zero-flux Neumann boundary conditions are imposed. The thermal conductivity, k, is assumed to be constant within the plane wall with a dimensionless value of $k = 75$. Thermal diffusivity α takes arbitrary value as solutions are independent.

In the case of the 1D-plane wall with different fixed temperatures (Fig. 6-1(a)), Dirichlet boundary conditions are used to represent the fixed temperature surfaces. At $x = 0$, the boundary is fixed to a temperature of $T_1 = 800$, and at $x = L$ the boundary is fixed to a temperature of $T_2 = 400$. The temperature field for $0 < x < L$ is initialized at a uniform $T = 600$. In the case of the 1D-plane wall with a heat source (Fig. 6-1(b)), a zero-flux Neumann boundary condition is imposed at $x = 0$ to represent the adiabatic surface. The uniform source $\dot{q}$ is fixed to a value of $\dot{q} = 1500$, such that $\frac{\dot{q}}{k}$ becomes 20. In order for the system to reach steady state, the right free surface at $x = L$ must remove energy at the same rate as the uniform source $\dot{q}$. As such, the Neumann boundary

condition of $-20 \times 256 = -5120$ is imposed at $x = L$. The temperature field for $0 < x < L$ is initialized at a uniform $T = 1000$. Total energies of the systems should be conservative such that average temperature remains $T = 1000$ after the temperature profile converges to steady state.

6.2. TEMPERATURE PROFILES AT STEADY-STATE

Figures 6-2(a) and (b) show the temperature profile across the computational domain at steady-state for both the implicit and explicit integration schemes. Numerical results provided by MEMPHIS are compared to the analytical solutions. Both numerical methods lead to similar results as compared to the analytical solutions.

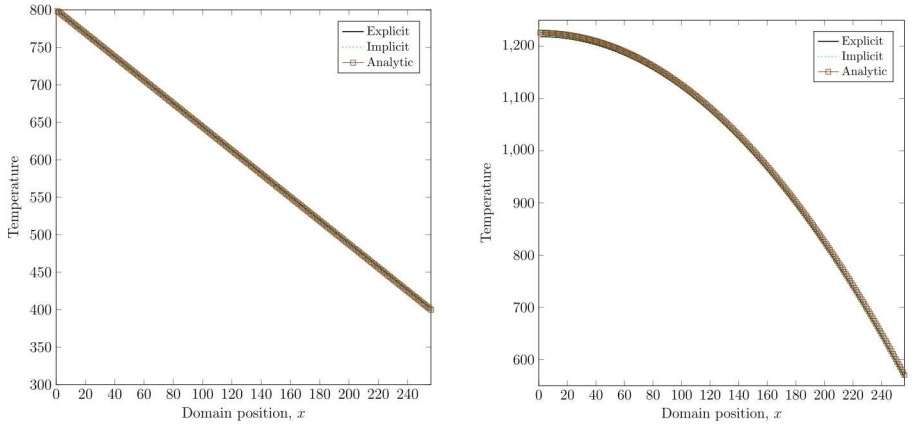

Figure 6-2. Temperature profile across the computational domain at steady-state in the case of (a) the 1D-plane wall with different fixed temperatures and, (b) the 1D-plane wall with a heat source.

7. SUMMARY

The goal of this exercise was to verify and validate the correctness, accuracy and precision of the models and numerical methods implemented into MEMPHIS. Computational results and comparisons to existing phase-field results have demonstrated that MEMPHIS is a robust and efficient phase-field capability to be used by the nanoscience and materials science community. As new models are implemented into MEMPHIS and its capabilities are extended, additional benchmark problems will complement its verification and validation suite of problems.

REFERENCES

[1] J.W. Cahn. On spinodal decomposition. *Acta Metall.*, 9(9):795–801, 1961.

[2] F.P. Incropera, A.S. Lavine, T.L. Bergman, and D.P. DeWitt. *Fundamentals of heat and mass transfer*. Wiley, 2007.

[3] A.M. Jokisaari, S.S. Naghavi, C. Wolverton, P.W. Voorhees, and O.G. Heinen. Predicting the morphologies of γ' precipitates in cobalt-based superalloys. *Acta Mater.*, 141:273–284, 2017.

[4] A.M. Jokisaari, P.W. Voorhees, J.E. Guyer, J. Warren, and O.G. Heinonen. Benchmark problems for numerical implementations of phase-field models. *Comput. Mater. Sci.*, 126:139–151, 2017.

[5] A.M. Jokisaari, P.W. Voorhees, J.E. Guyer, J. Warren, and O.G. Heinonen. Phase-field benchmark problems for dendritic growth and linear elasticity. *Comput. Mater. Sci.*, 149:336–347, 2018.

[6] A. Karma and W.-J. Rappel. Quantitative phase-field modeling of dendritic growth in two and three dimensions. *Phys. Rev. E*, 57:4323, 1998.

[7] J. A. Stewart and R. Dingreville. Microstructure morphology and concentration modulation of nanocomposite thin-films during simulated physical vapor deposition. *Acta Mater.*, in press.

[8] S. Yoon and A. Jameson. Lower-upper symmetric-gauss-seidel method for the euler and navier-stokes equations. *AIAA J.*, 26(9):1025–1026, 1988.

DISTRIBUTION

Hardcopy—Internal

Number of Copies	Name	Org.	Mailstop
1	Ryan Wixom	1881	1315

Email—Internal (encrypt for OUO)

Name	Org.	Sandia Email Address
Technical Library	01177	libref@sandia.gov

Sandia National Laboratories is a multimission laboratory managed and operated by National Technology & Engineering Solutions of Sandia LLC, a wholly owned subsidiary of Honeywell International Inc., for the U.S. Department of Energy's National Nuclear Security Administration under contract DE-NA0003525.